forum acusticum 2026
8-12 September · Graz, Austria

EFFECT OF BLADE TIP GEOMETRY ON THE NOISE SPECTRUM AND SOUND PRESSURE LEVEL OF FDM 3D-PRINTED DRONE PROPELLERS

I. Šantak[1], T. Uroić[1], J. Ivošević[2], K. Krajček Nikolić[2]
[1] *Faculty of Mechanical Engineering and Naval Architecture, Zagreb, Croatia*
[2] *Faculty of Transport and Traffic Sciences, Zagreb, Croatia*

This paper is a revised version of the authors' submitted manuscript that was peer-reviewed by at least two anonymous reviewers.

Abstract

Propellers are the dominant source of noise in drones, with the blade tip region playing a critical role due to high local flow velocities and strong aerodynamic interactions. In addition to overall sound pressure level, the spectral content of the emitted noise significantly influences human perception and annoyance.
This study investigates the effect of blade tip geometry on A-weighted sound pressure level with FAST time weighting (L_{AF}) and the frequency spectrum of fused deposition modeling (FDM) 3D-printed drone propellers in the hover regime. A baseline propeller geometry was modified by varying blade tip sweep angle ($-30°$, $0°$, and $+30°$) and tip chord length (baseline and 50% of the baseline). Acoustic measurements were conducted under zero inflow conditions over a rotational speed range from 5000 to 8000 RPM.
The results show that blade tip modifications influence both tonal and broadband noise components, leading to measurable differences in sound pressure level and spectral characteristics across operating conditions. In particular, certain configurations exhibit reduced variability in both acoustic and performance metrics, indicating more stable aerodynamic behavior.
These findings contribute to the understanding of aeroacoustic mechanisms in small drone propellers and support the development of low-noise propeller designs.

Keywords: *aeroacoustics, drone propellers, blade tip geometry, FDM, hover conditions*

1. Introduction

The rapid growth of drones has raised concerns regarding their acoustic impact, particularly in urban environments where operations occur close to observers. Rotor-generated noise is the dominant contributor to the acoustic signature of multirotor systems [1], [2], making propeller design a key factor in noise reduction.
Drone propeller noise consists of tonal and broadband components. Tonal noise is associated with the blade passing frequency (BPF) and its harmonics, while broadband noise originates from turbulent flow phenomena such as boundary layer interaction, vortex shedding, and trailing-edge noise [3], [4]. These mechanisms are strongly influenced by blade geometry and operating conditions.
The blade tip region is of particular importance, as it operates at the highest local velocities and is a major source of aerodynamic noise. Furthermore, modifications such as sweep angle and chord reduction can alter vortex formation and unsteady flow behavior, thereby affecting both tonal and broadband noise components [2].
Additive manufacturing, especially fused deposition modeling (FDM), enables rapid prototyping of customized propeller geometries. Despite limitations such as anisotropic material properties and surface roughness [5], [6], FDM is well suited for controlled experimental aeroacoustic studies.
While most studies focus on forward flight, hover conditions are highly relevant for many drone applications. In hover, the absence of inflow velocity emphasizes rotor-induced unsteady flow effects. Therefore, evaluating both sound pressure level (SPL) and thrust-to-power ratio (T/P), together with variability of acoustic measurements, provides a more comprehensive assessment of propeller performance.
This paper investigates the influence of blade tip geometry on the acoustic and aerodynamic performance of FDM 3D-printed drone propellers in hover. Variations in sweep angle and chord length are analyzed in terms of sound pressure level, frequency spectrum, and thrust-to-power ratio, with particular emphasis

Corresponding author: *ivor.santak@gmail.com.*

on variability as an indicator of unsteady aerodynamic behavior.

2. Materials and Methods

2.1. Propeller Material

All propellers were manufactured using fused deposition modeling (FDM) on a Prusa Core One 3D printer. A nozzle diameter of 0.25 mm and a layer height of 0.12 mm were used for all specimens, with default structural settings applied in PrusaSlicer.
The propellers were printed at an angle of 10° relative to the print bed without support structures. This orientation increases the effective interlayer bonding area and reduces the alignment of layer interfaces perpendicular to the primary tensile loading direction, thereby improving resistance to centrifugal stresses.
Prusa Buddy PLA filament was used as the printing material. It should be noted that FDM manufacturing inherently produces increased surface roughness compared to injection-molded propellers, which may affect boundary layer behavior and modify local airflow characteristics [7].

2.2. Propeller Geometry

A 9-inch diameter propeller with a 6-inch pitch was selected, as it represents a commonly used configuration for drone applications. The baseline propeller geometry was designed using blade element momentum (BEM) theory [8] and was kept constant across all designs in order to isolate the effect of blade tip modifications. A Clark Y airfoil was employed along the blade span, as it is commonly used in propeller design and exhibits favorable aerodynamic characteristics in the low-Reynolds-number regime.
To investigate the influence of blade tip geometry on acoustic and aerodynamic performance, modifications were applied exclusively to the blade tip region. This region is characterized by high local flow velocities and aerodynamic loading, and is therefore known to significantly contribute to noise generation [2]. The modified region corresponds to the outer 25% of the blade span. Moreover, the transition between the baseline blade and modified tip region was implemented smoothly to avoid geometric discontinuities.
The blade tip was modified by varying sweep angle and chord length. Two tip chord configurations were considered: the baseline chord length (12 mm) and 50% of the baseline value. Three sweep angles were investigated: −30°, 0°, and +30°, where negative angles correspond to backward sweep and positive angles correspond to forward sweep. This resulted in a total of six propeller configurations (Fig. 1).

2.3. Measurements

In addition to A-weighted sound pressure level (L_{AF}) and frequency spectra, thrust and electrical power were measured to evaluate propeller performance.
For each operating condition, the propeller was first allowed to reach the prescribed rotational speed and stabilize. Acoustic and performance data were then acquired continuously for 30 s. The sound analyzer

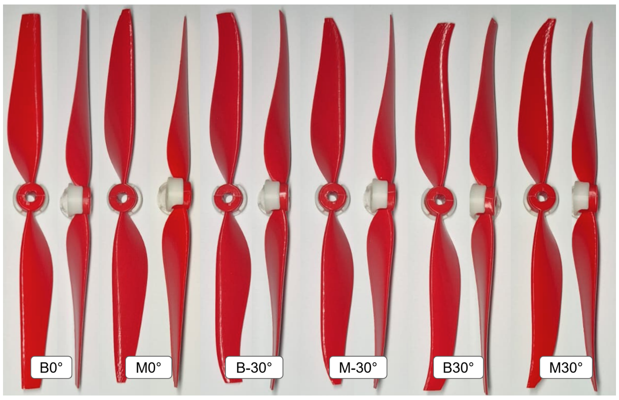

Figure 1: Top and side views of the investigated 3D-printed propeller geometries. Labels denote configuration and sweep angle, where B and M represent baseline and modified tip geometries, respectively, and 0°, −30° (backward sweep), and +30° (forward sweep) indicate the blade tip angle.

operated with FAST time weighting (125 ms time constant), and one L_{AF} value was logged at 1 s intervals. This provided 30 consecutive logged values for each propeller geometry and rotational-speed condition. The values were used to calculate the mean and temporal standard deviation. The one-third-octave spectra were evaluated over the same 30 s acquisition interval, which provided a stable estimate of the frequency-band levels. The L_{AF} values were measured directly by the sound analyzer as broadband A-weighted levels and were not reconstructed from the one-third-octave spectra; therefore, the one-third-octave spectral resolution did not affect their calculation.
The L_{AF} metric was selected instead of the equivalent continuous sound level (L_{Aeq}) to preserve short-term temporal variations in acoustic pressure. These variations are associated with unsteady aerodynamic phenomena, such as turbulence and vortex interactions, which contribute to broadband noise. In contrast, L_{Aeq} represents an energy-averaged value and does not capture this variability. This is particularly relevant in the present study, in which the standard deviation of L_{AF} is used as an indicator of flow stability.
The variability in derived quantities, such as the thrust-to-power ratio (T/P), was evaluated through propagation of the measured variability. The standard deviation of T/P was calculated assuming independent variations in thrust and power as:

$$\sigma_{T/P} = \sqrt{\left(\frac{1}{P}\sigma_T\right)^2 + \left(\frac{T}{P^2}\sigma_P\right)^2} \qquad (1)$$

where σ_T and σ_P denote the temporal standard deviations of thrust and electrical power, respectively.
Measurements were conducted in a rotational speed range from 5000 to 8000 RPM, with increments of 1000 RPM. The sound analyzer was positioned at a height of 2.5 m and at an angle of 45° relative to the

propeller axis, in the horizontal plane, at a distance of 1.5 m from the propeller. This configuration was selected to reduce ground reflection effects and to approximate free-field measurement conditions while maintaining a sufficient signal-to-noise ratio, consistent with common practices in outdoor aeroacoustic measurements [2], [9]. All acoustic and performance measurements were conducted using the stationary test rig described in Section 2.4, which was installed outdoors on a sport-aircraft runway. Testing was conducted under nighttime conditions to minimize background noise and wind disturbances (Fig. 2).

Figure 2: Experimental setup during testing.

2.4. Experimental Setup

The experimental setup used for acoustic and performance measurements is shown in Fig. 3. It consisted of a stationary test rig including a 500 W, 900 KV brushless motor used to drive the propellers, controlled via a VESC controller using a custom Python interface. Rotational speed was measured using a magnetic encoder, and a stroboscopic tachometer was used for validation, achieving an accuracy of ±3 RPM. Thrust was measured using integrated measurement electronics mounted within the motor holder, and electrical power was obtained from the VESC.

Acoustic measurements were performed using a Norsonic Nor140 sound analyzer (Class 1). Prior to each measurement series, the system was calibrated using a Norsonic Nor1251 acoustic calibrator (Class 1).

2.5. Environmental Conditions

Measurements were conducted under stable ambient conditions, with temperatures of 10–11°C, relative humidity of 58–62%, and wind speeds below 1 m/s, as reported by the nearest meteorological station.

Background noise was assessed during periods when the motor was not operating to establish a reference level for evaluating the signal-to-noise ratio. The measured background level was approximately 30.3 dB (L_{AF}), based on 30 samples, with a standard deviation of ±1.8 dB. This is at least 15 dB lower than the propeller noise across all operating conditions, indicating a negligible influence on the measured results.

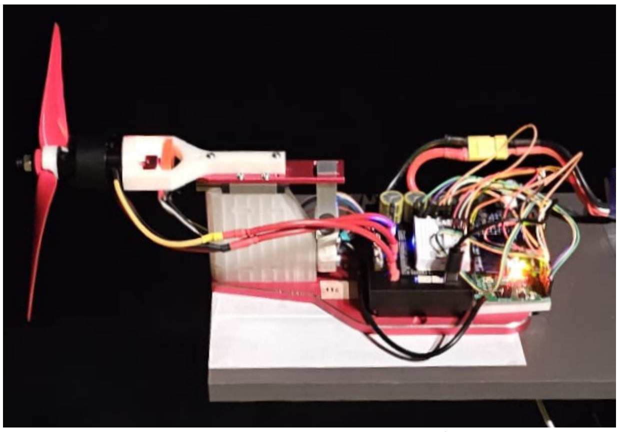

Figure 3: Motor holder with integrated rotational speed encoder and thrust measurement electronics used in the experimental setup.

Given the stable environmental conditions and the sufficient signal-to-noise ratio, environmental influences were not further treated, and no corrections for background noise or free-field geometric effects were applied.

3. Results and Discussion

The legend used in Figs. 4 and 5 distinguishes between baseline and modified propellers, as well as blade sweep angle. Negative sweep angles (−30°) correspond to backward sweep, while positive sweep angles (+30°) correspond to forward sweep.

3.1. Sound Pressure Level as a Function of Rotational Speed

The variation of A-weighted sound pressure level with FAST time weighting (L_{AF}) as a function of rotational speed is presented in Fig. 4. For all tested configurations, L_{AF} increases monotonically with increasing rotational speed, which is consistent with the increase in blade tip velocity and aerodynamic loading observed in previous drone rotor noise studies [2].

A comparison between baseline and modified geometries shows that the modified propeller consistently produces lower sound pressure levels across all tested rotational speeds, with reductions of approximately 1–3 dB depending on configuration. This indicates that blade tip modifications effectively reduce noise emission over the entire operating range.

3.2. Effect of Sweep Configuration

The influence of sweep configuration (0°, −30°, and +30°) on acoustic performance is evident in Fig. 4. The results show that the optimal sweep angle depends on both blade geometry and rotational speed.

For the baseline geometry, the backward-swept configuration (−30°) consistently produces the lowest L_{AF} across the investigated operating range, indicating a clear acoustic benefit of backward sweep in this case.

For the modified geometry, the trends are more dependent on rotational speed. The unswept con-

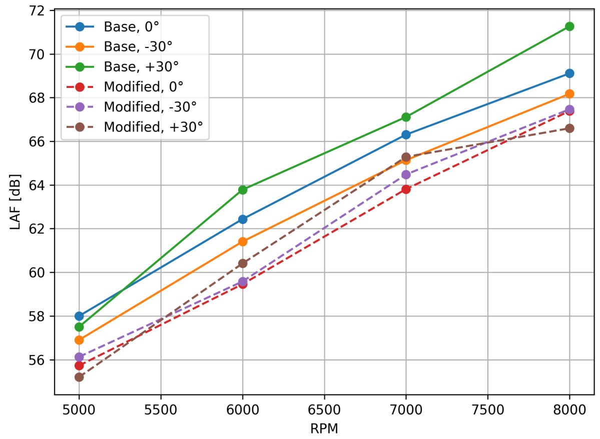

Figure 4: A-weighted sound pressure level with FAST time weighting (L_{AF}) as a function of rotational speed for baseline and modified propellers under three sweep configurations (0°, −30° backward sweep, and +30° forward sweep).

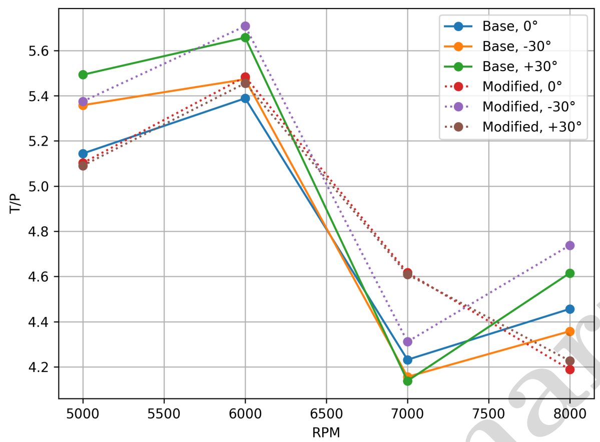

Figure 5: Thrust-to-power ratio T/P as a function of rotational speed for baseline and modified propellers under three sweep configurations.

figuration (0°) yields the lowest L_{AF} at 6000 and 7000 RPM, while the forward-swept configuration (+30°) produces lower sound pressure levels at 5000 and 8000 RPM.
These results indicate that the effect of sweep on noise generation is strongly coupled with blade geometry and operating conditions, rather than being governed by a single optimal configuration. This behavior is consistent with previous findings [2].

3.3. Efficiency Analysis

The thrust-to-power ratio T/P as a function of rotational speed is shown in Fig. 5. All configurations exhibit peak efficiency at intermediate rotational speeds (approximately 5000–6000 RPM), followed by a decrease at higher rotational speeds. This behavior is consistent with increased aerodynamic losses and nonlinear flow effects at higher loading conditions [8].

A more detailed comparison reveals that, for the −30° sweep configuration, the modified swept propeller exhibits higher efficiency than its baseline swept counterpart across all rotational speeds, except at the lowest tested speed.
Furthermore, when comparing sweep configurations, propellers with −30° sweep demonstrate higher efficiency than their 0° counterparts at lower rotational speeds (5000 and 6000 RPM), indicating a potential advantage of backward sweep in low-RPM operating conditions.
Overall, the differences in T/P between configurations remain moderate and depend on both sweep angle and rotational speed.

3.4. Variability and Measurement Stability

Variability provides additional insight into the stability of aerodynamic and aeroacoustic behavior beyond mean values. Figure 6 shows the standard deviation of both L_{AF} and T/P for the baseline and modified propellers.

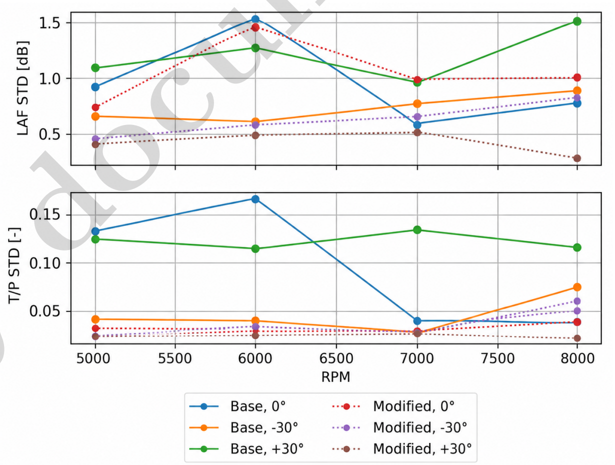

Figure 6: Variability of acoustic (L_{AF}) and performance (T/P) metrics as a function of rotational speed for baseline and modified propellers under different sweep configurations.

For the backward sweep configuration (−30°), the baseline propeller exhibits lower variability compared to its 0° and +30° counterparts at 5000 and 6000 RPM in both L_{AF} and T/P, indicating more stable operation in this regime.
Overall, the modified propellers with backward (−30°) and forward (+30°) sweep tend to show reduced variability compared to their baseline counterparts across most operating conditions.
A consistent reduction in variability in both L_{AF} and T/P provides stronger evidence of improved flow stability, as it suggests that both aerodynamic performance and noise generation are less affected by unsteady flow behavior. In contrast, reductions observed in only one metric may reflect differing sensitivities of the aerodynamic and acoustic responses to geometric modifications.

3.5. Frequency-Domain Analysis

Frequency-domain characteristics were analyzed for each operating condition using one-third-octave band spectra. The spectra are presented as median frequency-band sound pressure levels ($L_{f,50}$), corresponding to the 50th percentile of the measured levels within each frequency band over the acquisition interval. This representation provides a robust estimate of typical spectral content while reducing the influence of transient fluctuations.

For each rotational speed, spectra corresponding to different geometries were compared, focusing on tonal components associated with the blade passing frequency (BPF) as well as broadband noise contributions. The blade passing frequency, which defines the primary tonal component of rotor noise, is given by:

$$f_{\text{BPF}} = \frac{N_b \cdot \text{RPM}}{60} \tag{2}$$

where N_b is the number of blades and RPM is the rotational speed.

Although the one-third-octave representation does not resolve narrowband tonal peaks explicitly, tonal components can still be inferred from elevated levels in frequency bands corresponding to the expected BPF range. The interpretation of tonal behavior is consistent with classical rotor noise theory [10], [11], while the broadband content is consistent with established trailing-edge and turbulence-related noise models [3], [4].

Representative median frequency-band sound pressure level spectra at 6000 RPM are shown in Figs. 7–9 for the three sweep configurations. This rotational speed was selected as it represents a mid-range operating condition where both tonal and broadband noise contributions are clearly observable under stable conditions.

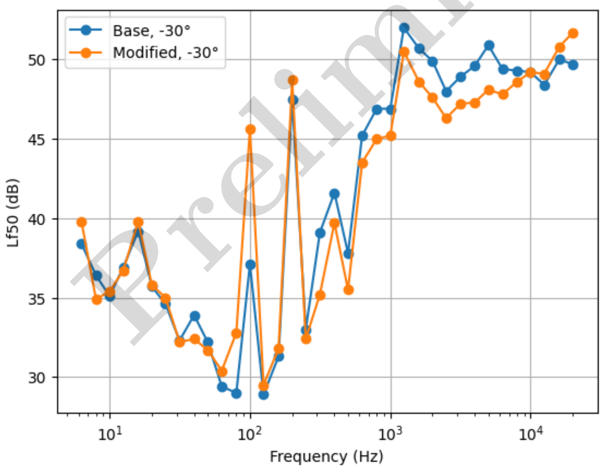

Figure 7: Median one-third-octave band sound pressure levels ($L_{f,50}$) for baseline and modified propeller geometries at 6000 RPM and $-30°$ (backward sweep) configuration.

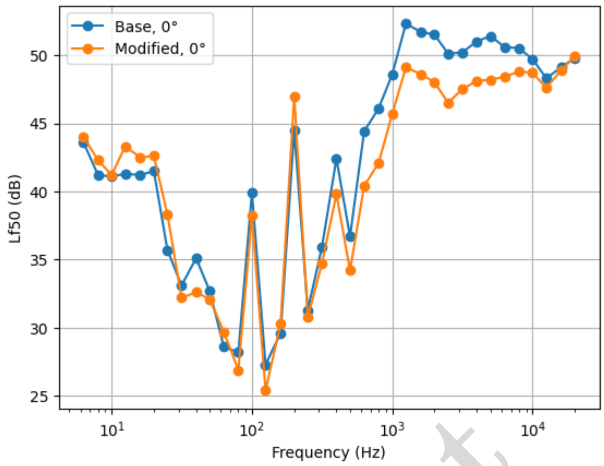

Figure 8: Median one-third-octave band sound pressure levels ($L_{f,50}$) for baseline and modified propeller geometries at 6000 RPM and 0° configuration.

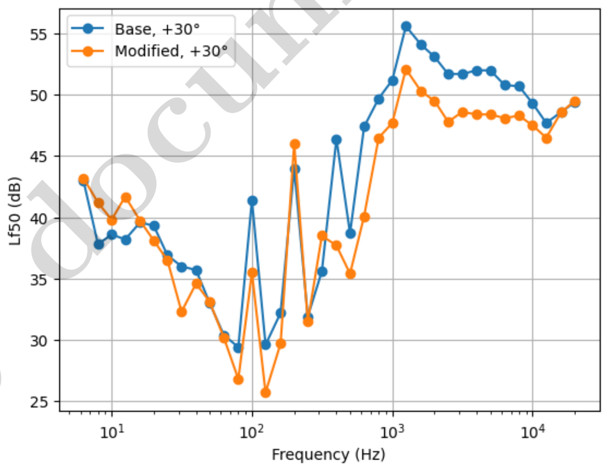

Figure 9: Median one-third-octave band sound pressure levels ($L_{f,50}$) for baseline and modified propeller geometries at 6000 RPM and $+30°$ (forward sweep) configuration.

The spectra indicate that geometric modifications influence both low- and high-frequency content. Differences between baseline and modified propellers are most pronounced in the mid- to high-frequency range, which is particularly relevant for human perception and annoyance[9]. In several configurations, the modified propeller exhibits reduced spectral levels over broad frequency ranges, consistent with the lower variability observed in time-domain measurements and suggesting improved flow stability.

In addition, the modified propeller exhibits slightly lower levels in the one-third-octave bands associated with the blade passing frequency across all sweep configurations, indicating a reduction in tonal noise components. However, since the modified geometries differ from the baseline in blade area, the present results do not allow the individual effects of this change to be isolated. Variations in blade area also affect aerodynamic loading, which directly influences tonal noise components. Therefore, definitive conclusions regarding tonal behavior cannot be drawn without further analysis.

These findings support the hypothesis that blade tip modifications can reduce unsteady aerodynamic phenomena associated with broadband noise generation, while also slightly affecting tonal noise related to periodic aerodynamic loading.

4. Conclusion

This study investigated the influence of propeller blade tip geometry on acoustic and aerodynamic performance through systematic experimental measurements and the results demonstrate that geometric modifications significantly affect both sound pressure level and spectral characteristics.

The modified propeller consistently exhibited lower sound pressure levels compared to the baseline configuration across all tested operating conditions. In addition, reduced variability was observed in both acoustic (L_{AF}) and performance (T/P) metrics, with the most consistent reductions occurring at 5000 and 6000 RPM for both forward ($+30°$) and backward ($-30°$) sweep configurations. These trends may indicate more stable aerodynamic behavior, although further investigation would be required to directly confirm the underlying flow mechanisms.

Furthermore, influence of sweep angle was found to be condition-dependent, with swept configurations generally reducing noise at lower rotational speeds, while differences became less consistent at higher speeds. The thrust-to-power ratio remained comparable between configurations, indicating that noise reductions were achieved without significant performance penalties.

Frequency-domain analysis showed that geometric modifications influence both broadband and tonal noise components. In particular, reductions in broadband noise were consistent with decreased variability. The results also indicate a potential reduction in tonal components associated with the blade passing frequency. However, further confirmation would require narrowband (FFT-based) analysis, as the present study is based on one-third-octave measurements.

Overall, the results highlight that blade tip geometry plays a key role in aeroacoustic performance. The findings suggest that targeted modifications can reduce noise while maintaining comparable efficiency, and that variability can serve as a useful indicator of aerodynamic behavior. These results support the development of low-noise drone propellers and provide a basis for further optimization studies.

5. Acknowledgments

The authors acknowledge the Laboratory for Aircraft Emissions at the Faculty of Transport and Traffic Sciences, University of Zagreb, for providing the Norsonic Nor140 sound analyzer and the Norsonic Nor1251 acoustic calibrator.

The authors also gratefully acknowledge Aeroklub Sisak for granting access to their airfield for the experimental measurements.

References

[1] J. Ivošević, E. Ganić, A. Petošić, and T. Radišić, "Comparative uav noise-impact assessments through survey and noise measurements," *International Journal of Environmental Research and Public Health*, vol. 18, no. 12, p. 6202, 2021.

[2] N. S. Zawodny, D. D. J. Boyd, and C. L. Burley, "Acoustic characterization and prediction of representative, small-scale rotary-wing unmanned aircraft system components," in *Proceedings of the American Helicopter Society (AHS) Annual Forum*, West Palm Beach, FL, USA, 2016.

[3] T. F. Brooks, D. S. Pope, and M. A. Marcolini, "Airfoil self-noise and prediction," NASA, Reference Publication 1218, 1989.

[4] M. Roger and S. Moreau, "Back-scattering correction and further extensions of amiet's trailing-edge noise model. part 1: Theory," *Journal of Sound and Vibration*, vol. 286, no. 3, pp. 477–506, 2005.

[5] S. H. Ahn, M. Montero, D. Odell, S. Roundy, and P. K. Wright, "Anisotropic material properties of fused deposition modeling abs," *Rapid Prototyping Journal*, vol. 8, no. 4, pp. 248–257, 2002.

[6] A. R. Torrado Perez, D. A. Roberson, and R. B. Wicker, "Fracture surface analysis of 3d-printed tensile specimens of novel abs-based materials," *Journal of Failure Analysis and Prevention*, vol. 16, no. 1, pp. 154–164, 2016.

[7] H. Schlichting and K. Gersten, *Boundary-Layer Theory*, 9th ed. Berlin: Springer, 2017.

[8] J. G. Leishman, *Principles of Helicopter Aerodynamics*, 2nd ed. Cambridge: Cambridge University Press, 2006.

[9] A. Christian and R. Cabell, "Initial investigation into the psychoacoustic properties of small unmanned aerial system noise," NASA, Technical Memorandum NASA/TM-2017-219429, 2017.

[10] M. V. Lowson, "The sound field for singularities in motion," *Proceedings of the Royal Society A*, vol. 286, no. 1407, pp. 559–572, 1965.

[11] F. Farassat, "Derivation of formulations 1 and 1a of farassat," NASA, Technical Memorandum NASA/TM-2007-214853, 2007.